Measurement Science and Standards

Shielding factor of protective eyewear

Ernesto Mainegra-Hing, Hong Shen, Malcolm McEwen

Ionizing Radiation Standards

Report PIRS-2350 June 2017

CNSC Report designation RSP-651.1

The provision of this report and results, or the use of any particular equipment described herein does not represent an endorsement by the National Research Council of such equipment for the measurement of ionizing radiation.

National Research Council Canada Conseil national de recherches Canada

EXECUTIVE SUMMARY

Experimental and theoretical data have been obtained for a range of standard protective (non-leaded) eyewear types in a number of different photon and electron radiation beams. It was found that the shielding factor provided by such eyewear is generally very small. For a 16 keV (30 kVp) beam this factor is around 1.3, decreasing to unity as the mean photon energy approaches 100 keV. The shielding factor of the Sr-90/Y-90 beam is more significant, around 2.5-3 for the eyewear types tested.

Multiple investigations were carried out, using different experimental geometries and comparing measurement data with very detailed Monte Carlo simulations, to confirm the validity of the experimental data obtained. No significant difference was seen in the shielding properties of the three materials tested – polycarbonate, CR-39 and Trivex. Differences in the attenuation properties of the different eyewear types were measurable but these were correlated with the thickness of the shielding material used for the eyewear lenses. Variations in the attenuation of the eyewear as a function of the angle of incidence of the radiation beam were seen but these were not large enough to indicate a preference for one type over another or specify an angular dependence to the overall shielding factors.

The excellent agreement between measurements and Monte Carlo simulations provides a basis for more complex investigations mimicking realistic radiation protection scenarios. Although anthropomorphic phantoms are available for physical dose measurements, the flexibility that the Monte Carlo approach provides, in terms of varying geometries, material compositions and incident beam energy, makes it the preferred option for future investigations.

TABLE OF CONTENTS

LIST OF TABLES AND FIGURES

1. BACKGROUND

The lens of the eye is one of the most radiosensitive tissues in the body and the main health effect of concern is its opacification, which is termed cataract in its advanced stages. To prevent the incidence of radiation-induced cataracts, nuclear regulatory bodies worldwide set dose limits for the lens. Currently the dose limit prescribed by the CNSC's *Radiation Protection Regulations* for the lens is 150 mSv per one year dosimetry period for Nuclear Energy Workers (NEW) and 15 mSv per calendar year for members of the public, or persons who are not NEWs.

Recently, a number of human epidemiological studies and experimental animal-based studies have suggested that the development of cataracts may occur following exposure to significantly lower doses of ionizing radiation than previously considered. Taking into consideration all of the information, and in alignment with the recommendations of the ICRP, the CNSC is proposing the following amendments to the *Radiation Protection Regulations*:

- to change the equivalent dose limit for the lens of an eye for a Nuclear Energy Worker from the current limit of 150 mSv to 50 mSv in a one-year dosimetry period
- to add a new dose limit for the lens of an eye for a Nuclear Energy Worker of 100 mSv in a five-year dosimetry period

While the process to amend the Regulations is on-going, it is recognized that stakeholders would benefit from regulatory guidance to assist in enhancing the protection of the lens of the eye of workers from ionizing radiation.

The purpose of this research project is to assist CNSC staff in developing regulatory guidance in the area of reducing dose to the lens of the eye. Specifically, the study is focused on researching the shielding factor offered by traditional safety glasses and prescriptive eyewear that are commonly used in the industry, or readily available for purchase and use.

2. SCOPE OF WORK

The scope of work covered experimental and theoretical investigations of the shielding factor offered by a representative range of eyewear in radiation beams that are typical of exposure situations in CNSC's regulated activities. The specific investigations, *as envisioned at the outset of the project*, are given in Tables I and II.

Table I. Experimental investigations of eyewear shielding factors

1. kV x-rays	
Energies	Sufficient energies in the range 15 keV to 65 keV (effective energy) to characterize the energy dependence of shielding factors Medium filtration bremsstrahlung beam qualities.
Measurements (a)	Simple attenuation measurements Form - planar sheet, three materials - polycarbonate, CR-39, Trivex Measurements to be carried out in-air, shielding material placed approximately 2 cm in front of detector (approximating glasses-eye separation). Detector: standard ionization chamber with sensitive size consistent with eyeball Measurements at multiple angles in range 0-90 degrees
Measurements (b)	Characterization of eye wear shielding Form – at least 5 types of eyewear readily available in Canada and meeting CSA Z94.3 standard Measurements to be carried out in-air, eyewear placed approximately 2 cm in front of detector (approximating glasses-eye separation). Detector: standard ionization chamber with sensitive size consistent with eyeball Measurements at multiple angles in range 0-90 degrees
2. Sr-90/^{90}Y beta source	
Energy	Standard spectrum for Y-90/Sr-90 beta source (end-point energy = 2.28 MeV)
Measurements (a)	Same as for kV x-rays above
Measurements (b)	Same as for kV x-rays above

Table II. Theoretical (Monte Carlo) investigations of eyewear shielding factors

1. kV x-rays	
Energies:	Sufficient energies in the range 15 keV to 65 keV (effective energy) to characterize the energy dependence of shielding factors Simulated beams should match as closely as possible the experimental beams
Calculations (a)	Simple attenuation measurements Form - planar sheet, three materials - polycarbonate, CR-39, Trivex Simulated geometry to match experimental measurements "Detector": dose to detector will be scored with and without the shielding material present.
Calculations (b)	Simulation of eye wear shielding Modelling of the complex 3-D geometry of eyewear is beyond the scope of this project. Simplified models based on 2-D curvature (e.g., portion of a cylinder) will be used.
2. Beta source	
Energy	Standard spectrum for Y-90/Sr-90 beta source (end-point energy = 2.28 MeV).
Calculations (a)	Same as for kV x-rays above
Calculations (b)	Same as for kV x-rays above, augmented with mono-energetic electron beams in range 700 keV to 10 MeV.

During the investigation there were a number of deviations from the original statement of work, as laid out in Tables I and II. These deviations were discussed and agreed with CNSC staff and the main ones are as follows:

i) the number of photon energies was reduced from 5 to 4 because initial measurements with planar sheets indicated that no additional information would be gained from the additional photon energy of 50 keV;

ii) the range of sheet thicknesses used was increased to provide additional attenuation data beyond standard eyewear thicknesses;

iii) the range of measurement angles used for testing the planar sheets was reduced because of experimental limitations;

iv) the number of measurement angles used for testing eyewear was increased to improve the characterization of eyewear shielding;

v) for x-ray beams dose to detector's sensitive volume rather than air-kerma was scored in the MC calculations for direct comparison with measurements.

3. EXPERIMENTAL INVESTIGATIONS

3.1 Materials

Three materials were investigated: Polycarbonate (Makrolon®[1]), CR-39[2], and Trivex (TVX31)[2]. Polycarbonate is the standard material used in non-prescription eyewear, whereas the lenses for prescription safety glasses can be all three materials. The respective base monomers for three materials are bisphenol-A, diethyleneglycol bis allylcarbonate (ADC) and urethane. Because CR-39 and Trivex are generally only available as prescription lenses, all the types of eyewear investigated in this work had polycarbonate lenses. The investigations of the planar sheets were designed to highlight any material-specific differences.

Although polycarbonate is available from a number of suppliers with different tradenames (e.g. Lexan®, Zelux®) the chemical composition is nominally the same, and therefore the radiation shielding properties should be independent of the specific source.

The density of the planar sheets was measured and found to be:

Polycarbonate:	ρ = 1.15 g cm^{-3} (± 0.5 %)
CR-39	ρ = 1.27 g cm^{-3} (± 2.4 %)
TVX31	ρ = 1.07 g cm^{-3} (± 1.5 %)

The larger uncertainty for the CR-39 density appeared to be due to variations in thin (1 mm) sheets but these are not generally used for eyewear.

The polycarbonate sheets were available in multiples of 1.15 mm and 3.25 mm; the CR-39 in multiples of 1.00 mm and 3.25 mm; and the TVX31 in multiples of 3.25 mm.

Six types of non-prescription eyewear were tested in this investigation and are shown in Figure 1. The intention was to test a realistic range of eyewear easily available in Canada, rather than capture a complete cross-section of types in current use. The testing of these particular types does not imply that they are superior for the purpose of radiation shielding, or even that they are recommended for normal situations. The cost of these types is in the range $3 to $25. Referring to Figure 1, Types #1 and #4 are perhaps the most common in laboratory environments; type #2 represents a design where the frame constitutes a larger fraction of the total shielding area; type #3 is specifically marketed for women, and types #5 and #6 can be considered higher-end “fashion” eyewear. The specific supplier of the polycarbonate for each eyewear type was not determined.

[1] Manufactured by Bayer
[2] Base material manufactured by PPG, Pittsburghm PA, in sheet from RTP Company, Winona, MN

Figure 1. Photographs of the six types of eyewear investigated in this project. As can be seen, these eyewear types show some significant differences in terms of curvature and lens size.

The manufacturers and model numbers (if available) of the eyewear types are as follows:

#1 = North "Visitor"
#2 = Pyramex "Emerge"
#3 = Stanley "Ladies"
#4 = Uvex (Honeywell)
#5 = Dakota "Indoor/Outdoor"
#6 = Dakota "MG"

The thickness of the lens portion of each type of eyewear was measured using a Mitutoyo precision thickness gauge, and the results are shown in Table III. The uncertainty on the measurements is estimated to be ± 0.1 mm.

Table III. Thickness of lens material in protective eyewear investigated.

Eyewear	Minimum thickness (mm)	Maximum thickness (mm)
#1	2.1	2.3
#2	2.2	2.3
#3	1.7	2.2
#4	2.1	2.9
#5	1.5	2.5
#6	1.7	2.1

The minimum thickness was generally found close to the hinge and the maximum thickness was between the centre of the lens and the nosepiece. In contrast to these thicknesses, a pair of prescription glasses (polycarbonate lens) was also measured and the thickness was in the range 3-7 mm, significantly greater. CSA Z94.3 provides the minimum thickness for prescription lenses to be consistent with the standard.

It is useful to define a “standard thickness” for comparing the different materials and, combining the available thicknesses of planar polycarbonate sheet with the data in Table III, this was chosen to be 2.3 mm.

3.2 Experimental set up – kV x-rays

The detector chosen for the kV x-ray measurements was an NE2571 Farmer-type ionization chamber[3], with a nominal volume of 0.6 cm^3 and an air cavity dimension of approximately 24 mm x 7 mm. This type of chamber is used for reference dosimetry in radiation therapy, has a well-established energy response and long-term stability. The ionization chamber was connected to a Keithley 35617 electrometer[4] and the polarizing voltage was set to 300 V.

The measurements were made using the NRC x-ray facility, consisting of two constant potential, stabilized x-ray tubes capable of generating potentials in the range 10 kV to 50 kV and 50 kV to 300 kV ((Phillips MCN-101 and COMET MXR-320 tubes respectively). The kVp and filtration are both readily varied and were chosen to give the required effective energies, shown in Table IV. The air kerma rate at the ionization chamber was in the range 50 mGy min^{-1} to 80 mGy min^{-1}, dependent on the energy.

Table IV. X-ray beam parameters

Tube kVp	Filter[†]	HVL	E_{eff} (keV)
30	0.51 mm Al	0.39 mm Al	15.7
50	1.79 mm Al	1.44 mm Al	25.0
80	4.13 mm Al	3.56 mm Al	35.4
135	0.39 mm Cu	0.60 mm Cu	64.8

[†] This is in addition to the inherent filtration of the x-ray tube.

The experimental set up for the planar sheet measurements is shown in Figure 2 and that for the eyewear testing in Figure 3.

[3] Manufactured by NE Technology Ltd, Beenham, UK
[4] Keithley Inc, Cleveland, OH

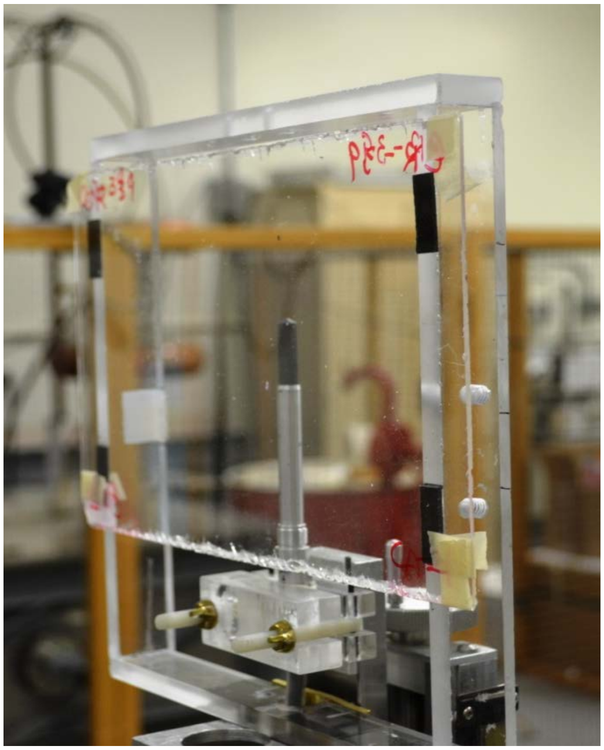

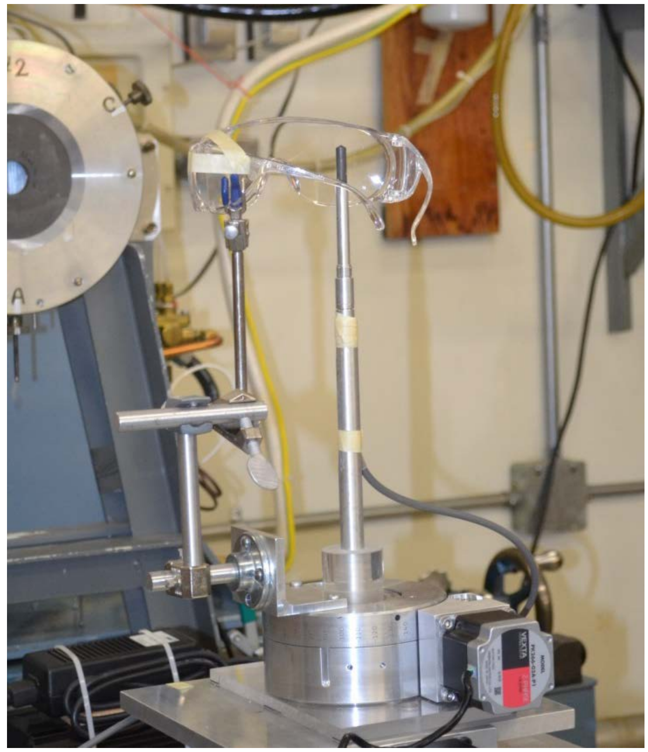

Figure 2 (left). Experimental set up for x-ray measurements. The diameter of the collimated x-ray beam is 90 mm at the position of the chamber, so all the large-mass structures (chamber holder, square frame) are outside the primary beam. The photograph shows multiple sheets of 1 mm thick CR-39 sheets positioned between the ionization chamber and the x-ray tube.

Figure 3 (right). Experimental set up for eyewear testing in x-ray beam. The collimator for the x-ray beam can be seen at the left-hand side, providing a 90 mm diameter beam at a source-detector distance of 1 m. The chamber is mounted in the centre of a Velmex[5] rotating stage and the glasses are positioned so that the chamber is approximately where the eye would be. The eyewear can be automatically rotated from the control room, speeding-up the data acquisition process.

3.3 Experimental set up –Sr-90/Y-90 beta source

The detector chosen for the Sr-90 measurements was an IBA FC-65G[6] Farmer-type ionization chamber. This chamber is very similar in design to the NE2571 chamber used for the x-ray measurements. The ionization chamber was connected to a Standard Imaging Supermax electrometer[7] and the polarizing voltage was set to -300 V.

[5] Velmex Inc, Bloomfield, NY
[6] IBA Dosimetry Gmbh, Schwarzenbruck, Germany
[7] Standard Imaging, Middleton, WI

The majority of measurements were made using a PTW T48010[8] check source of nominal activity 20 MBq (2003). It was chosen because of its availability and the simplicity of incorporating it into the experimental geometries required for the investigation. However, the low activity of this source meant that the source-detector distance had to be very short (~ 5 cm), to provide a measurable signal. Even with this short distance the measured ionization current was in the range 100 fA to 500 fA, which meant that leakage (non-radiation) currents could have a significant effect. However, the SI Supermax electrometer is designed to eliminate the effect of such leakage currents and the FC65-G chamber has been shown previously to exhibit intrinsic leakage currents in the range 3-10 fA.

A rotating-source geometry was developed for the Sr-90 measurements (in contrast to the rotating-shield geometry necessary in the x-ray set up). This is shown in Figures 4 and 5. The reason for the manual apparatus used here (rather than the automated Velmex system used for x-rays) is that it was simpler to keep the two experiments (kV x-rays and Sr-90) completely separate.

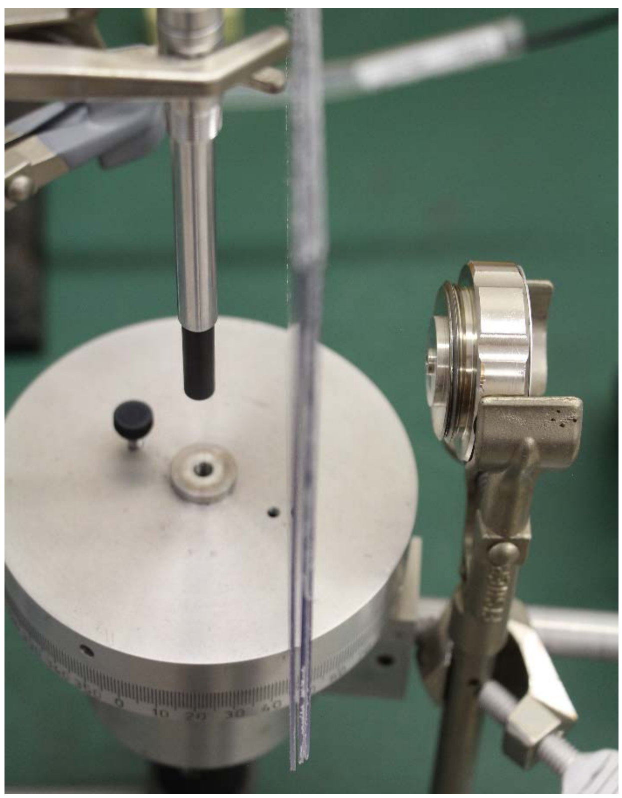

Figure 4. Experimental setup for Sr-90 measurements. The ionization chamber is centred on the rotating stage and the Sr-90 source is concentrically mounted. Rotation measurements without any shielding in place confirmed the concentricity, with ionization chamber readings constant at that 2 % level with source rotations of > 120°. Also shown in the figure are multiple thicknesses of shielding material. The source-chamber distance is approximately 50 mm.

[8] PTW, Freiburg, Germany

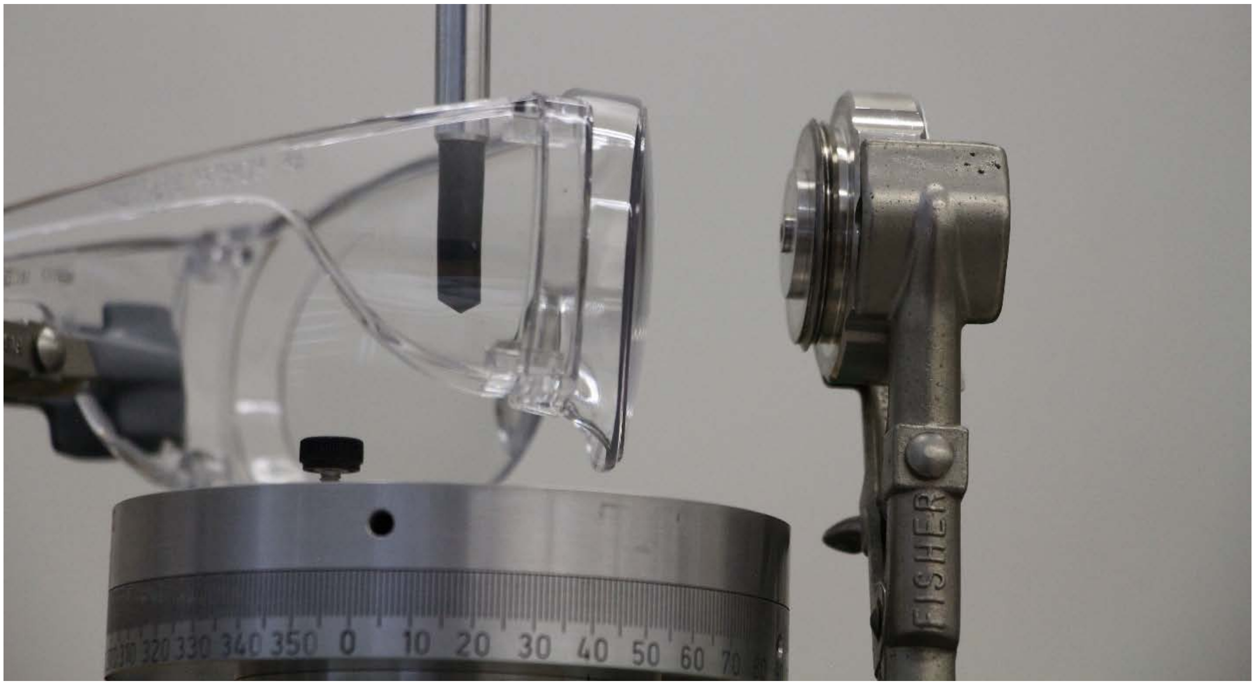

Figure 5. Experimental set up for eyewear shielding measurements. The same geometry was used as for the planar sheet measurements (source and chamber remained in same position). Each pair of glasses was positioned with the ionization chamber in the centre of one eyepiece, at approximately 2 cm from the detector. This geometry allowed the source to be rotated to irradiate the chamber through the side-frame as well. The relative angular indication of the source position can be seen in this image.

3.4 Definition of parameters

Shielding factors are determined from the ratio of absorbed dose to gas, D_{gas}, values with and without attenuating materials. D_{gas} is the dose to the sensitive volume of the ionization chambers used for the measurements, delivered by x-ray beams, a ^{90}Sr beta source and mono-energetic electron beams. D_{gas} is related to the measured signal M by the relationship

$$D_{gas} = \left(\frac{W}{e}\right)_{gas} \frac{M}{m_{gas}} \quad (1)$$

where "gas" in the case of the ionization chambers used in this study refers to air under reference conditions (T = 22 $^{\circ}$C, P = 101.325 kPa), m_{gas} is the mass of air in the chamber's sensitive volume, and $\left(\frac{W}{e}\right)_{gas}$ is the energy required to produce an ion pair in air. M is the fully-corrected signal from the detector (taking account of factors such as polarity and ion recombination, leakage and environmental reference conditions).

Since $\left(\frac{W}{e}\right)_{gas}$ is considered to be a constant, there is a direct relationship between D_{gas} and the detector signal *M*, and the ratios of these quantities for different attenuator thicknesses should be identical. For this reason in what follows, D_{gas} ratios refer to MC results while *M* ratios refer to the measurements.

Attenuation, *A(d),* due to a material of thickness *d* is defined as

$$A(d) = \frac{D_{gas(d)}}{D_{gas}(0)} = \frac{M(d)}{M(0)} \qquad (2)$$

Although attenuation is most commonly used to characterize photon beams, for consistency in presenting the results, the same term is used for all radiation types.

Shielding Factor, *SF(d)* is defined as the inverse of the attenuation:

$$SF(d) = \frac{1}{A(d)} \qquad (3)$$

Attenuation values for this investigation are in the range 1.00 (no attenuation of the incident beam) to 0.1, with corresponding shielding factors of 1.0 to 10.0.

4. MONTE CARLO INVESTIGATIONS

The irradiation setups were simulated using the Monte Carlo (MC) method and compared to the corresponding measurements to establish the accuracy of the calculations for the situations under investigation and perform sensitivity studies of the effect of different parameters on the results. This validation will prove useful beyond the present project, where more complex scenarios (e.g., anthropomorphic phantoms) are better suited to Monte Carlo simulations, rather than measurements.

The 2016 development branch of the EGSnrc MC simulation toolkit was used for the calculations. EGSnrc is an open source package developed and maintained at the NRC and it is currently distributed via github under the AGPL 3.0 Public License.

4.1 Material composition

An important ingredient of every MC simulation is accurate knowledge of the materials present in the geometry. For the three materials of interest, the composition of the polycarbonate and CR-39 monomers can be found in the literature, but this is not the case for Trivex. On an educational website one can find a statement about the manufacturing process being based on polyurethane chemistry enriched with additional nitrogen. Since no further information was available, the polyurethane composition was taken from the EGSnrc data base. Note that polyurethane composition can vary considerably depending on the method used in production, therefore the material simulated is referred to as “Trivex-equivalent”. Table V shows the composition of these materials as used in the simulations.

Table V. Material composition as used in the Monte Carlo simulations.

Material	ρ (g cm^{-3})[1]	Elemental composition (%)			
		H	C	N	O
Polycarbonate	1.15	5.5	75.6	-	18.9
CR-39	1.27	6.6	52.6	-	40.8
Trivex-equivalent	1.07	9.3	55.2	8.0	27.5

[1] The densities, as given above in section 3.1 were used in the simulations.

4.2 Monte Carlo set up – kV x-rays

The NRC x-ray tubes for low and medium energies are modelled using BEAMnrc, an EGSnrc application-generator tailored for the simulation of linear accelerators and x-ray tubes. BEAMnrc applications for these x-ray tubes, compiled as shared libraries, are used as particle sources for the C++ EGSnrc application **`cavity.`** Default transport parameters are used in the simulations and particles are followed until their energy falls below a cut-off of 1 keV. The application is used to model the NE2571 Farmer-type ionization chamber and compute ratios of D_{gas} with and without the attenuating sheets of materials *on-the-fly*. Variance reduction techniques such as photon splitting and range rejection with Russian roulette are used to increase calculation efficiency. A large number of histories are simulated in order to achieve 1σ statistical uncertainties in the dose ratios of less than 0.1 %. Figure 6 shows how the Monte Carlo geometry can accurately model the actual experiment.

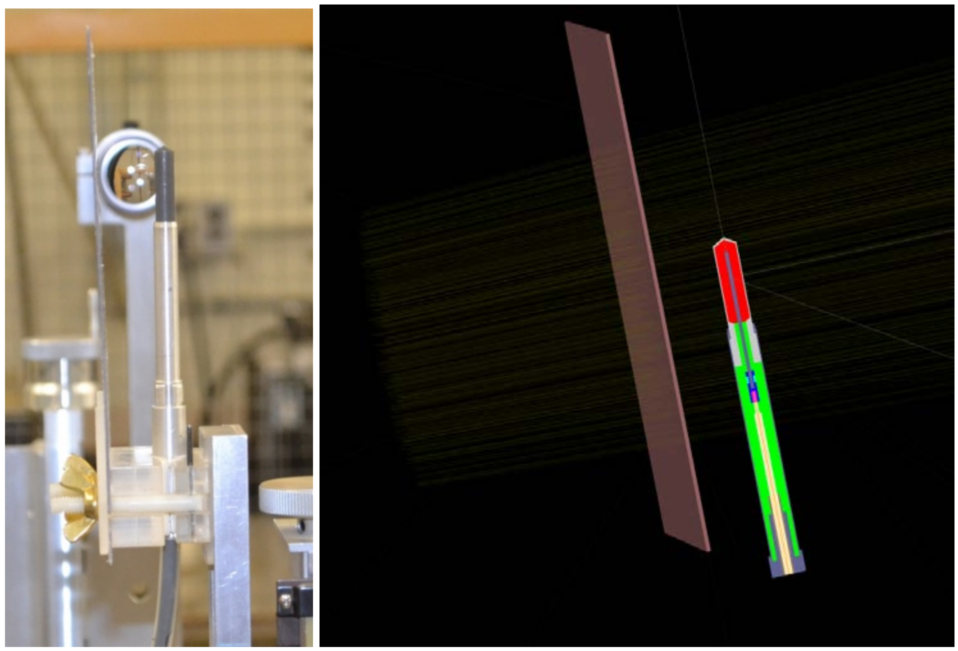

Figure 6. Monte Carlo model of the experimental x-ray geometry. On the right, one can see the geometrical model of the experimental setup used for measuring attenuation from planar sheets of shielding materials using a NE2571 Farmer-type ionization chamber (left). Particle tracks for the x-ray beam are shown, indicating the actual field size of the beam.

Since in practice the x-ray tubes cannot be rotated to investigate the effect of the beam angle of incidence on the attenuation, the sheets of materials were rotated around the chamber axis by the desired angle. This is equivalent to rotating the x-ray tube, provided the x-ray field is uniform and large enough at the point of measurement. The simulations are performed using the same approach, and this is shown in Figure 7.

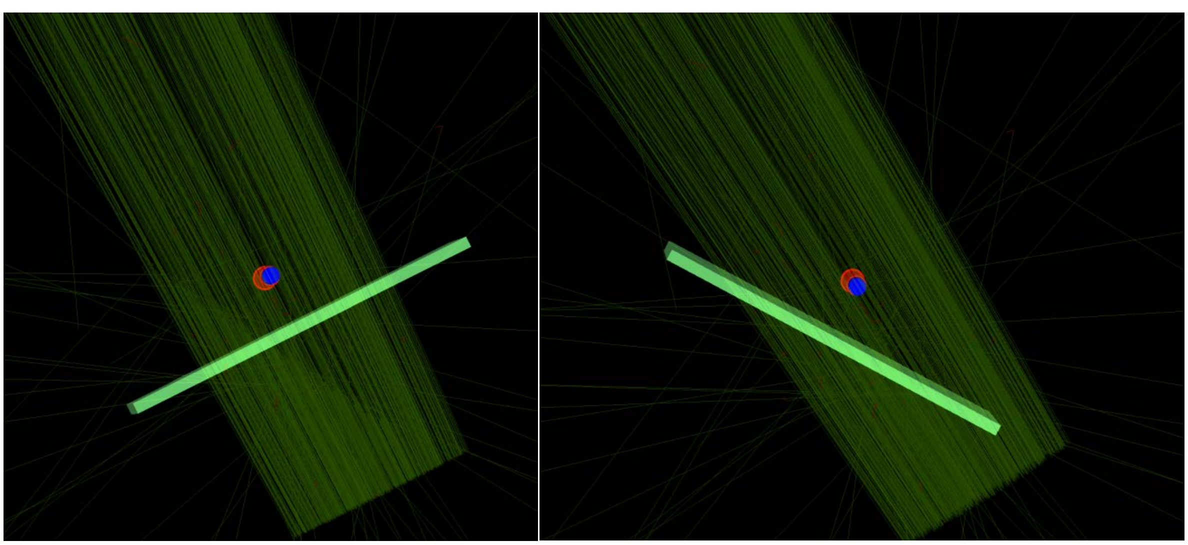

Figure 7. Simulated setup used in the measurement of the angular effect on attenuation. An initial positioning of the sheet is shown on the left, and a 60^{o} rotation is shown on the right.

The EGSnrc application **`cavity`** can be used to extract the x-ray spectrum from a BEAMnrc simulation. Figure 8 shows the spectra for the x-ray beam qualities used in this project.

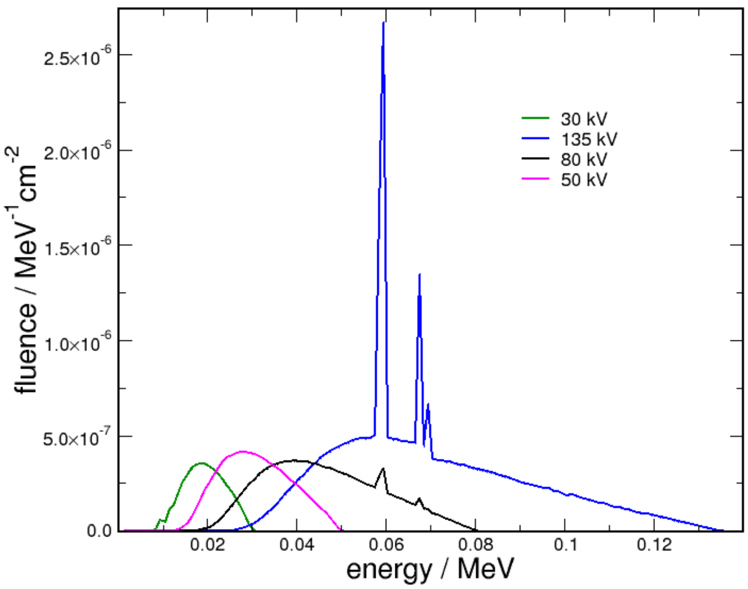

Figure 8. Monte Carlo calculated x-ray spectra of the four x-ray beams used in this investigation

A comparison of the MC spectra to the actual spectra for all qualities is shown in Table VI by means of the effective energy E_{eff} and the half-value layer HVL (the experimental HVL values were determined previously). These quantities are obtained from the calculated spectra using a binary search algorithm to find the thickness of material that reduces the air-kerma to half its value, *i.e.*, the HVL. The data used by this algorithm, such as mass attenuation and mass energy absorption coefficients, are taken from the EGSnrc package for consistency.

Table VI. Comparison of experimental and simulated effective energy and HVL values for x-ray beams.

Potential	**E_{eff} (keV)**		**HVL**	
kV	Experimental	Monte Carlo	Experimental	Monte Carlo
30	15.7	15.95	0.39 mm Al	0.39 mm Al
50	25.0	25.11	1.44 mm Al	1.42 mm Al
80	35.4	37.26	3.56 mm Al	3.85 mm Al
135	64.8	63.48	0.60 mm Cu	0.57 mm Cu

The reason behind using D_{gas} rather than the simpler quantity air-kerma, K_{air}, is due to the fact that the x-ray beam quality changes as it is attenuated by sheets of different thicknesses. Hence the calibration coefficient N_K for these qualities is not known. One possibility is to use as an approximation the N_K calibration curve as a function of the effective energy E_{eff} and extract N_K values by interpolation using MC-calculated E_{eff} for these beams and each sheet thickness. The accuracy of the N_K values determined using this approximation can be seen in Figure 9, where they are compared with values obtained for the 30 kV x-ray beam from a pure MC approach based on the relationship

$$N_K = \left(\frac{W}{e}\right)\frac{1}{m_{gas}}\frac{K_{air}}{D_{gas}} \tag{4}$$

As can be seen, the approximated N_K values differ by about 1% from the MC value for no shielding material. As the beam hardens, this difference decreases to around 0.5 %. It is therefore clear that for the purposes of this investigation, the two approaches are equivalent, but the direct MC method is preferable as it is independent of any measurements.

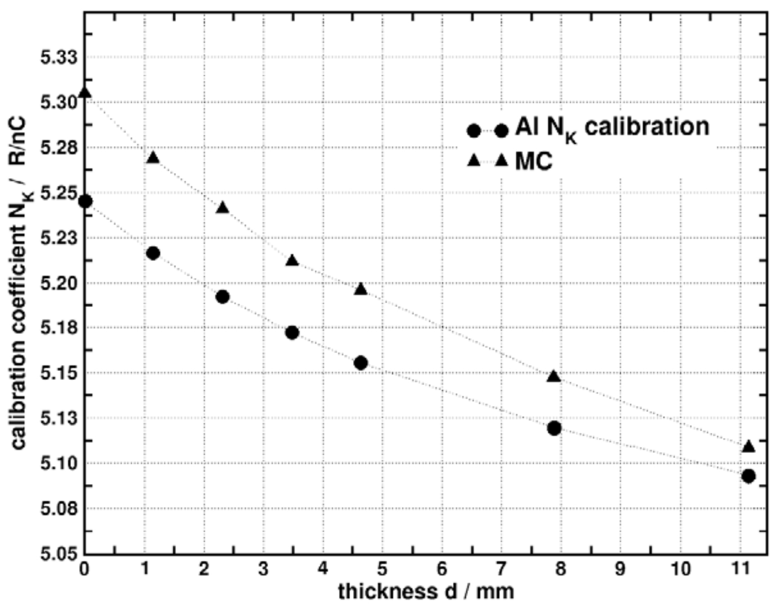

Figure 9. Estimated values of the air-kerma calibration coefficient N_K obtained using two different methods. Circles show values interpolated from the calibration curve measured at NRC using MC calculated values of E_{eff}. triangles show values obtained from direct MC simulation of the NE2571 ionization chamber response and the calculation of the air-kerma.

4.3 Monte Carlo set up –Sr-90/Y-90 beta source

The technical information for the PTW T48010 check source, as provided in the operating manual, was not detailed enough to construct an accurate model using EGSnrc. Specifically, missing information included material composition inside the active volume of the source and the characteristics of the source encapsulation. Through private communication with the manufacturer, PTW, information regarding exit window thickness and material was provided, making it possible to build an approximated model of the source. This geometrical model of the source is shown in Figure 10 as part of the measuring setup including a sheet of polycarbonate and the Farmer-type ionization chamber used for the measurements. Electron tracks visualization allows confirmation of the correct definition of the radionuclide source.

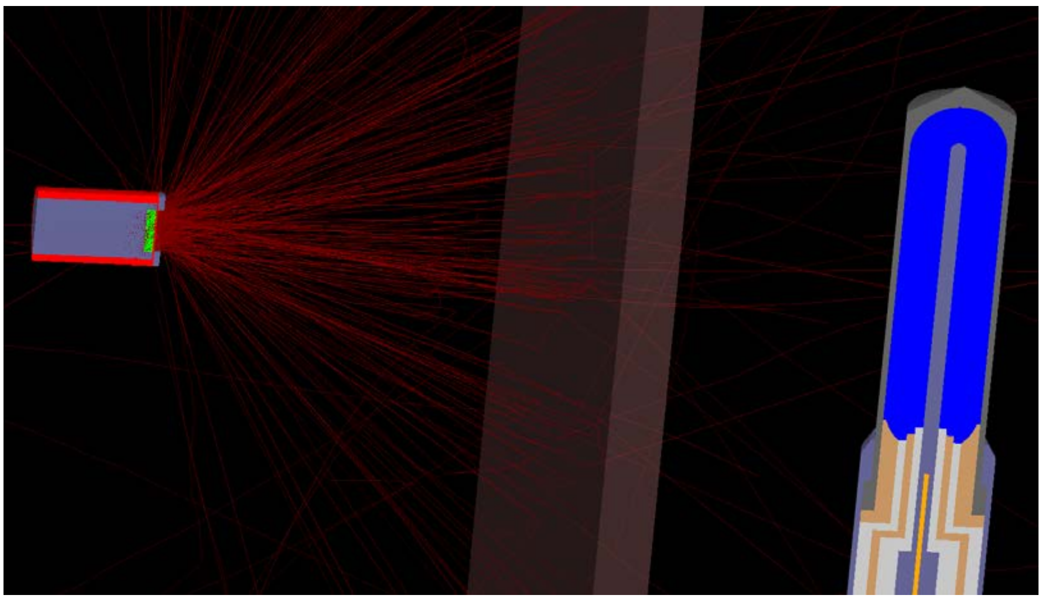

Figure 10. Monte Carlo model of the PTW ^{90}Sr check source T48010 shown on the left as part of the irradiation setup of planar sheets. A detailed model of the Farmer-type ionization chamber is shown on the right.

Calculations to determine the effect of angular incidence of the electron beam corresponded to the experimental arrangement, with the source rotating around the chamber's central axis (Figure 5).

4.4 Monte Carlo calculations for mono-energetic electron beams

Calculations for mono-energetic electron beams were performed using the same setup used for the Sr-90 beta source. A circular parallel beam of 1.5 mm radius positioned at 5 cm from the detector was incident on a polycarbonate sheet positioned at 1.7 cm from the detector. Only calculations for polycarbonate were undertaken as it was shown experimentally that for other materials the shielding factor scaled with density. The left panel of Figure 11 shows electron tracks for a 0.7 MeV electron beam and a Farmer-type ionization chamber.

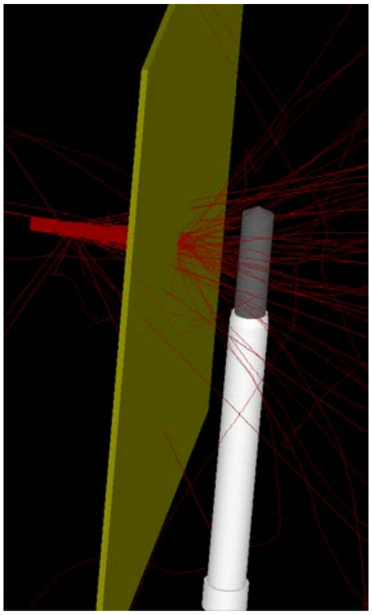

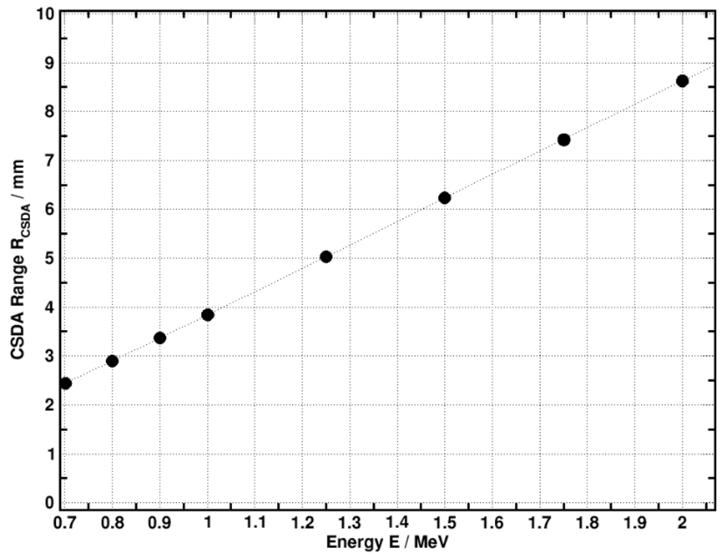

Figure 11. Left: Setup used for calculations of mono-energetic electron beams. **Right:** Range of electrons as a function of energy from the NIST ESTAR data base.

The energy range from 0.7 MeV to 10 MeV was divided in 22 intervals, where from 0.7 MeV to 1 MeV a 0.1 MeV energy interval is used while from 1 MeV to 10 MeV a 0.5 MeV energy interval is selected. An 11-point grid varying from 0 to 3 mm thickness on a logarithmic scale is used to cover the range of thicknesses of commonly used eyewear types.

A quick estimate of the shielding factor for electron beams can be obtained from a graph showing the variation of the electron range as a function of the energy. The CSDA (Continuous Slowing Down Approximation) range R_{CSDA} as function of the electron energy is shown in Figure 11 on the right. According to this graph, a 3 mm polycarbonate sheet will stop all electrons with energies below 0.8 MeV.

4.5 Monte Carlo eyewear models

Detailed geometrical modelling of different eyewear models is beyond the scope of this work. Instead, simplified eyewear models are obtained by measuring the chord length and the perpendicular distance from the centre of the chord to the centre of the glasses for type # 3 which has a nearly-circular curvature.

Two polycarbonate eyewear models were used for the MC calculations, one made out of a cylindrical slice and the other using a spherical slice. The cylindrical model will be curved only in the radial dimension while the spherical model will be curved in both dimensions. Figure 12 shows these models with a Farmer-type ionization chamber positioned at about 2 cm from the glasses, as was done for the measurements.

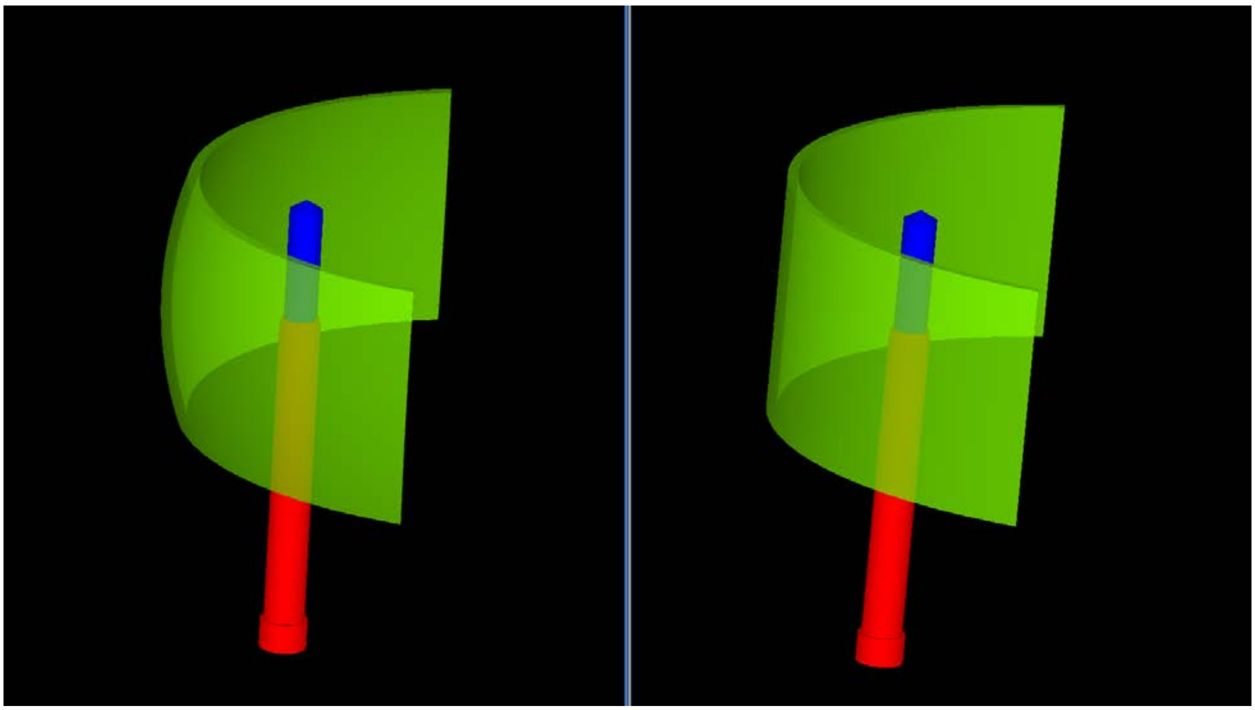

Figure 12. Monte Carlo eyewear models using a spherical slice (left) and a cylindrical slice (right) are shown here relative to their position in front of a Farmer-type ionization chamber. The chamber is placed at 2 cm from the glasses, centred on the right half of the glasses resembling the center of the right lens.

The rotation of the Sr-90 check source for the angular effect study is demonstrated in Figure 13 for -45^o, 0^o, and 45^o.

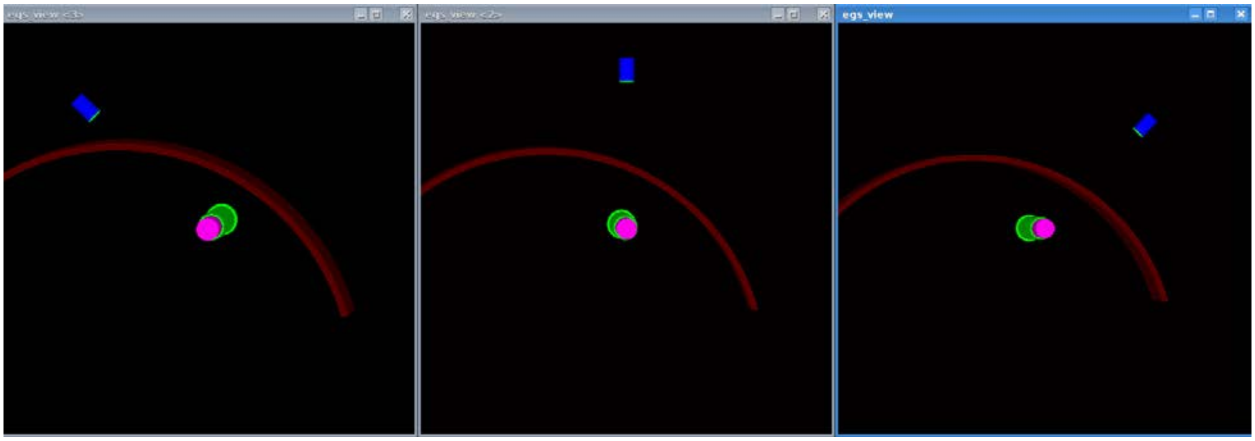

Figure 13. Top view of the Monte Carlo cylindrical eyewear model with the Sr-90 check source at three different angles. The ionization chamber is centred on the right half of the glasses at 2 cm. The chamber is viewed at a slight angle, with a pink thimble and green stem.

5. RESULTS

The findings presented in this section make use of the definitions of attenuation and shielding factor from section 3.4.

5.1 Planar sheets – effect of energy and absorber thickness

Figures 14 shows the attenuating properties of the three materials in kV x-ray beams and Figure 15 summarizes the energy dependence for a 2.3 mm polycarbonate sheet.

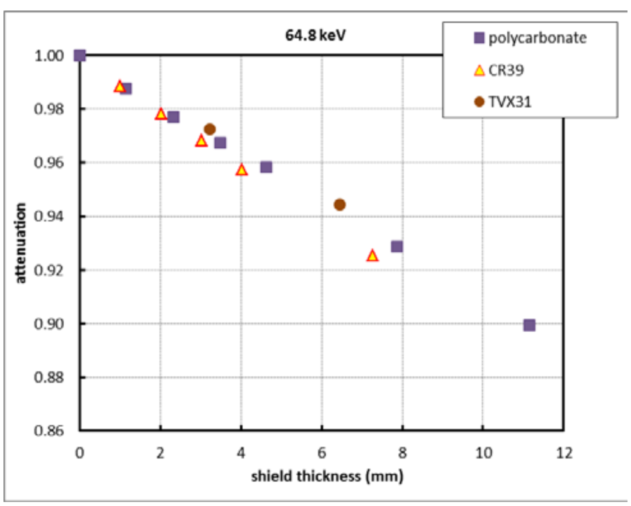

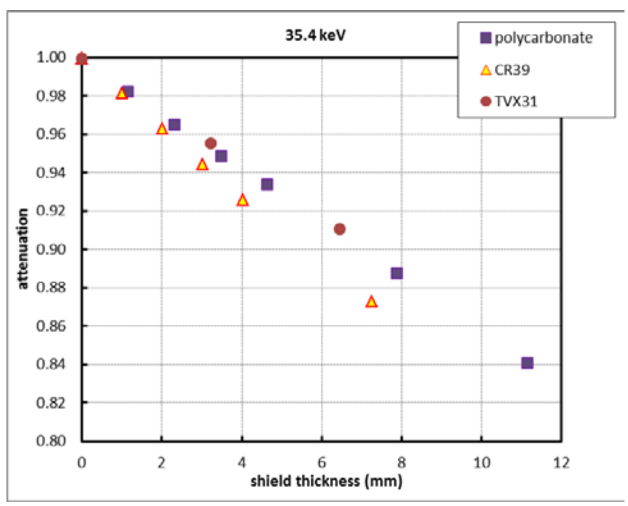

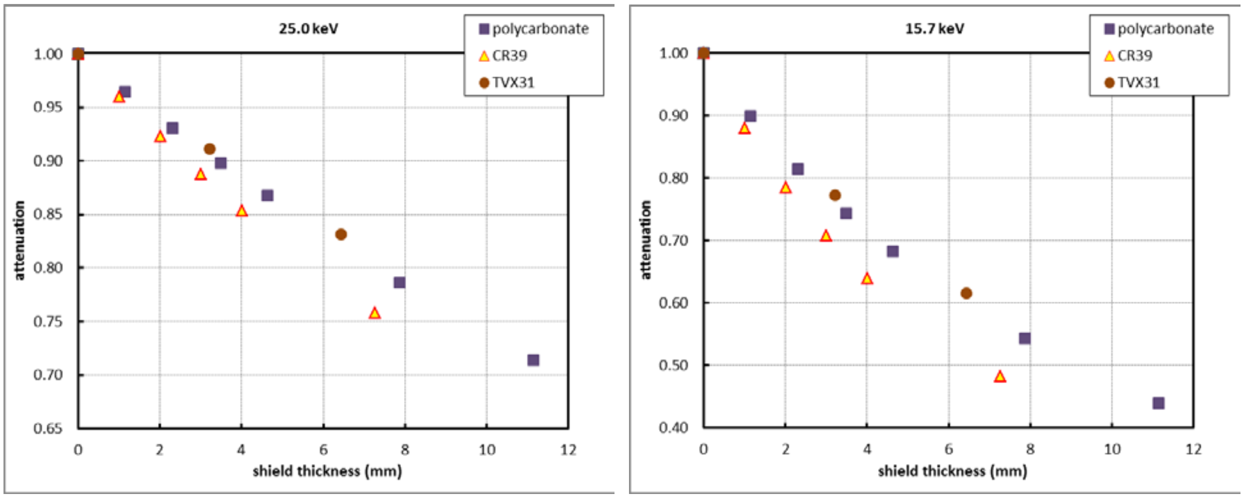

Figure 14. Attenuating properties of the three materials investigated as a function of material thickness and photon energy. The polycarbonate sheets were available in multiples of 1.15 mm and 3.25 mm; the CR-39 in multiples of 1.00 mm and 3.25 mm; and the TVX31 in multiples of 3.25 mm. Uncertainties bars of the same order symbol size.

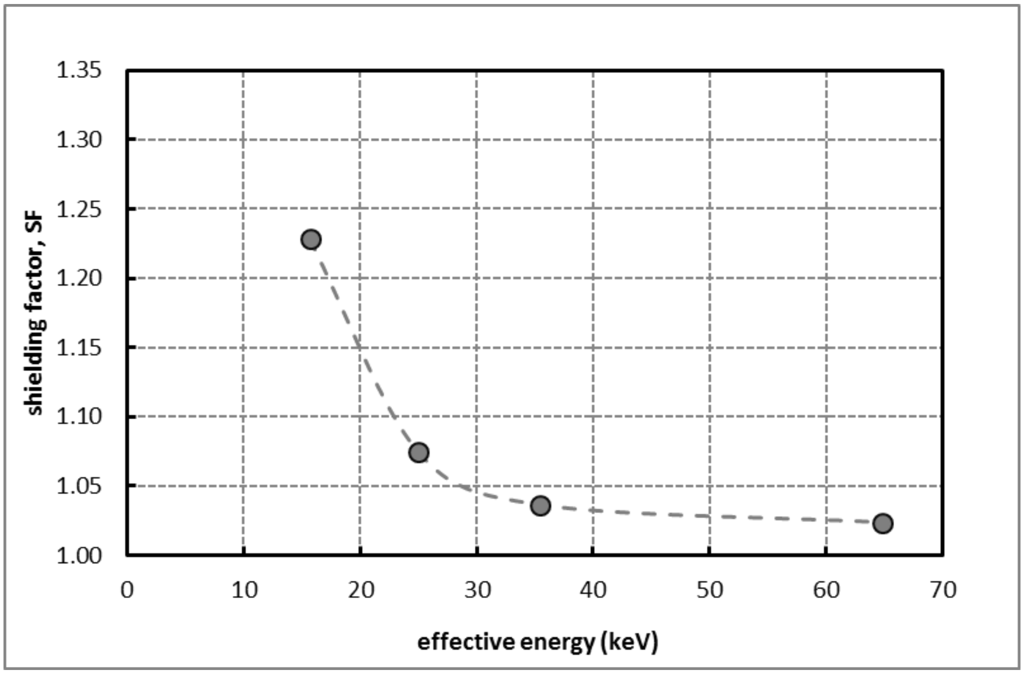

Figure 15. Variation in shielding factor (1/attenuation) as a function of energy for a 2.3 mm polycarboate sheet.

The range of thicknesses shown in Figure 14 spans the typical range for eyewear (up to 3 mm for non-prescription, perhaps as great as 6 mm for prescription lenses). One can see that the attenuation cannot be considered significant for any of the materials, except for the lowest energy x-ray beam (30 kVp), where a standard thickness (defined here as 2.3 mm) provides a shielding factor (= 1/attenuation) of around 1.2 (Figure 15).

The increased shielding provided by the CR39 material is due to the higher density (10 % greater than that of polycarbonate). The close matching of TVX31 with polycarbonate, despite the different densities suggests an additional atomic-number effect relating to the different monomer bases.

5.2 Planar sheets – effect of rotation

It is expected that the only effect of rotating planar sheets with respect to the radiation source is that the beam will traverse a longer path. Measurements were made with the Sr-90 source to confirm this and the results are shown in Figure 16. The source was rotated as in Figure 4, the size of the polycarbonate sheets and the small source-detector distance limiting the range of angles to 0° to 45°.

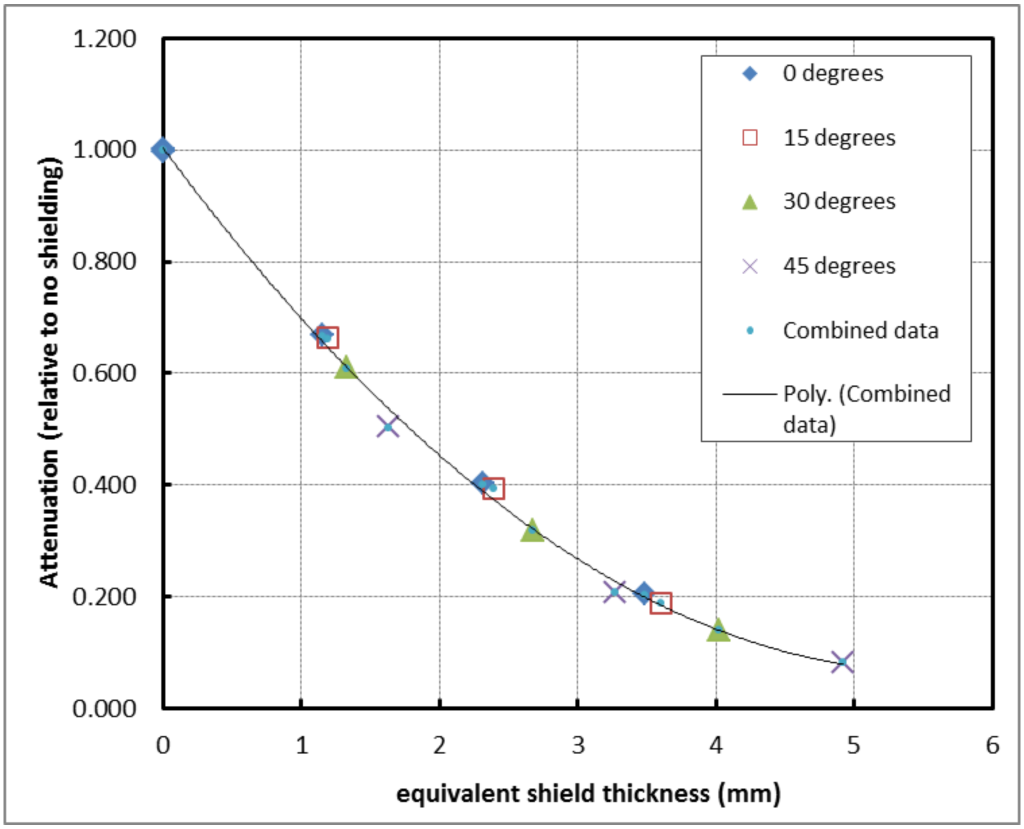

Figure 16. Effect of angle of beam relative to polycarbonate sheets on attenuation of Sr-90 beam. Equivalent shield thickness = physical thickness / cosine(angle of incidence). The fit is a 2^{nd}-order polynomial.

Some of the variation around the combined curve fitting, seen in Figure 16, is due to experimental uncertainties but one can also see a slight difference in the shape of the response curve for different angles. This is a second-order effect and likely due to differences in scattered radiation as a function of angle. However, for the purposes of this study one can use the linear thickness traversed by the radiation beam for calculating the shielding factor.

The range of sheet thicknesses is less than for the x-ray beams due to the increased shielding. For a typical thickness of 2.3 mm, the shielding factor for polycarbonate is around 2.5. A limited set of measurements were made with the other two materials and the results were consistent with the x-ray data (see Table A.1 in Appendix A). Although the difference in shielding factor is measurable for the three materials, it is small and for radiation protection guidelines, when considering the shield thicknesses found in eye wear, one could, to first order, ignore the material dependence.

5.3 Planar sheets – effect of geometry

Since the geometry in Figure 4 (source close to operator) is not typical of all field situations, a sensitivity study using a second higher-activity Sr-90 source was performed. The NRC BSS2 irradiator[9] was used for this study and the source-detector distance (SDD) was 310 mm, compared to 50 mm for the results in Figure 16. However, the geometry was constrained to a beam perpendicular to the shielding material. The polycarbonate sheet was placed at the same position relative to the detector as for the first Sr-90 source and the same ionization chamber was used. The results are shown in Figure 17.

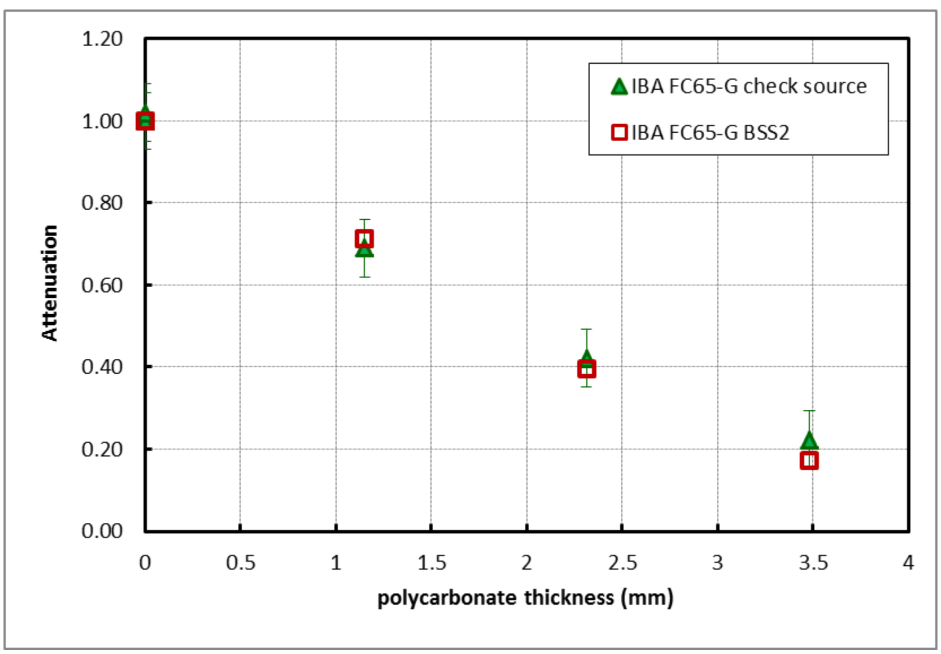

Figure 17. Comparison of attenuation with two different geometries using two different Sr-90 sources.

[9] Manufactured by PTW, Freiburg, Germany

As can be seen, the difference in results between the two setups is less than 5 %, similar to the differences seen for repeat setups of the geometry used in Figure 4 (and as indicated by the uncertainty bars in Figure 17). This data suggests that the shielding factor would be the same for a “real-life” scenario, where the source is more than 1 m from the detector.

A second sensitivity study was carried out, using the same BSS2 setup, into the effect of the position of the absorber relative to the detector, (i.e., investigating the effect of eyewear moving on the face). With the source-detector distance kept fixed the absorber material was moved over a wide range of distances. The results are shown in Table VII.

Table VII. Variation in shielding factor due to position of absorber relative to detector, source-detector distance maintained at 310 mm.

d[1] (mm)	$I_{chamber}$ (pA)	Shielding factor
----[2]	0.164	1.00
20	0.117	1.41
60	0.108	1.52
160	0.093	1.75
20	0.117	1.41

[1] distance between 1.15 mm sheet of polycarbonate and the centre of the IBA FC65-G ionization chamber
[2] measurement without any absorber present

As can be seen, the dependence of the shielding factor on the source-absorber distance is small. For an extreme variation in the eye-to-eyewear distance of 2 cm the change in shielding factor is only 4 %, which is not considered significant given the measurement uncertainties of around 5 %. This set of measurements was then repeated for the setup with the Sr-90 check source (as in Figure 4) and the results are shown in Table A.2 in the Appendix. For that geometry, a 2 cm change in the absorber position relative to the detector results in a change in the shielding factor of 30 %. These results show the same trend as the data in Table VII, in that as the absorber-detector distance increases, the transmitted intensity is reduced. The higher sensitivity to position for the small source-detector distance is likely due to the effect of scattered radiation.

The data in Tables VII and A.2 indicate that the data obtained with the eyewear positioned at approximately 2 cm from the detector can be considered the “worst” case in terms of the shielding effect of the eyewear.

5.4 Validation of experimental results with Monte Carlo calculations

5.4.1 Planar sheets – x-rays

The calculated attenuation due to irradiation with kV x-ray beams incident perpendicularly on the sheets is compared with experimental values for all three materials in Figure 18. The largest difference is observed for Trivex and the 30 kV x-ray beam and it amounts to about 5% for a thickness of 4.6 mm. Assuming exponential attenuation, a 1.5% error in the density would be responsible for a 1.2% variation in the attenuation. Moreover, as mentioned above, the composition of the monomer for Trivex is not known and an approximate composition (of polyurethane) has been used for the simulations. The graph on the lower right corner of Figure 18 shows the attenuation properties of all three materials. The results are consistent with the experimental findings, with CR-39 showing the largest linear attenuation, and polycarbonate and Trivex-equivalent giving similar results.

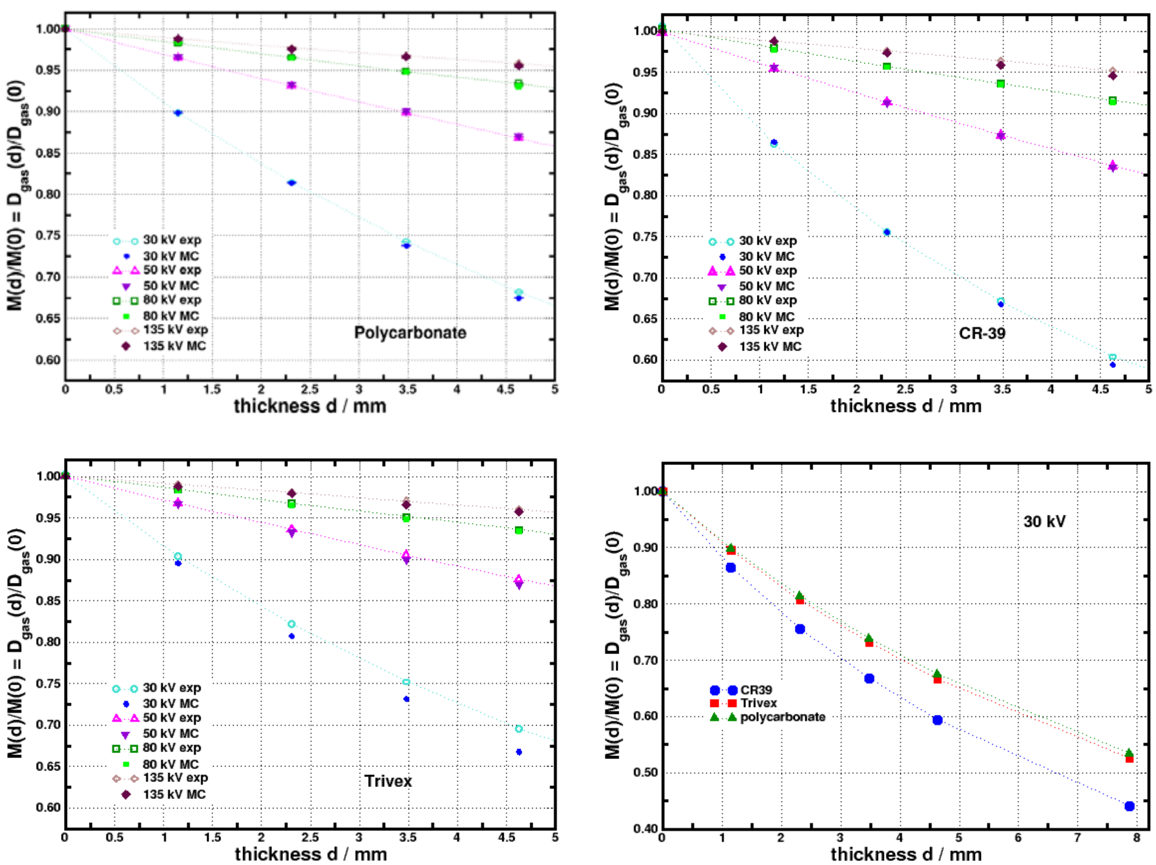

Figure 18. Comparison between experiment and MC calculations of attenuation due to kV x-ray beams for different materials. Graph on the lower right corner shows MC calculated attenuation properties of the different materials for the 30 kV x-ray beam. The "kV" values refer to the generating potential, see Table VI. Note that for the MC calculations, the material modelled is strictly "Trivex-equivalent" with a chemical composition based on a polyurethane monomer but using the measured material's density.

The effect of changing the angle of the source relative to the attenuating sheet was investigated using Monte Carlo calculations and, as for the experimental Sr-90 measurements in Figure 16, it was found that the change in shielding factor with angle was simply due to the increased path-length traversed by the radiation.

5.4.2 Planar sheets – Sr-90/Y-90 beta source

Simulations were performed using two different types of ionization chambers - a Farmer-type FC65G and a plane-parallel PTW Markus ionization chamber - for the situation with polycarbonate sheets. As shown in Figure 19, there is satisfactory agreement with the measurements performed with a Farmer-type IBA FC65-G ionization chamber. The lack of detailed information about the PTW48010 source adds to the uncertainty budget, and hence, the 8% local difference at the largest thickness lies within the combined uncertainties. Figure 18 also indicates that there is not a significant dependence on the chamber type used.

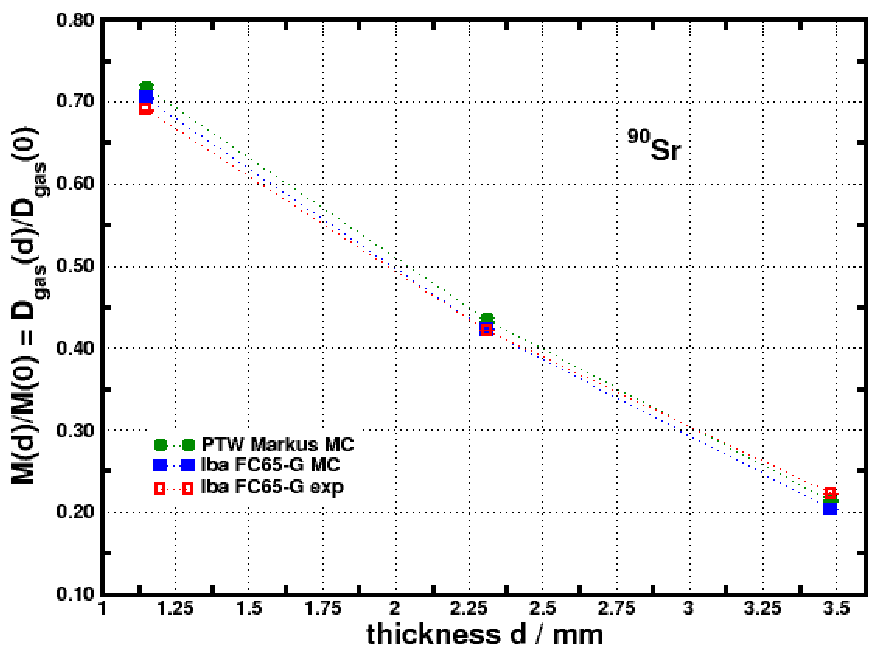

Figure 19. Comparison between experiment and MC calculations of the attenuation due to polycarbonate of the PTW ^{90}Sr check source T48010. Two different ion chambers are modelled and this data is compared to measurements with a Farmer-type FC65-G.

5.4.3 Attenuation of mono-energetic electron beams in the 0.7 to 10 MeV energy range.

As pointed out in section 4.4, most electrons with energies below 1 MeV will be fully stopped by a 3 mm layer of polycarbonate. Shielding curves for electron beams of different energies, as described in section 4.4, are shown in Figure 20.

To allow evaluation of the shielding for other thicknesses and energies, the MC values are fitted to an analytic expression that includes an attenuation term given by an exponential function and a constant scatter term. According to this model, attenuation A as function of the thickness d can be obtained as

$$A(d) = A_0 \cdot e^{-A_1 d} + A_2 \tag{4}$$

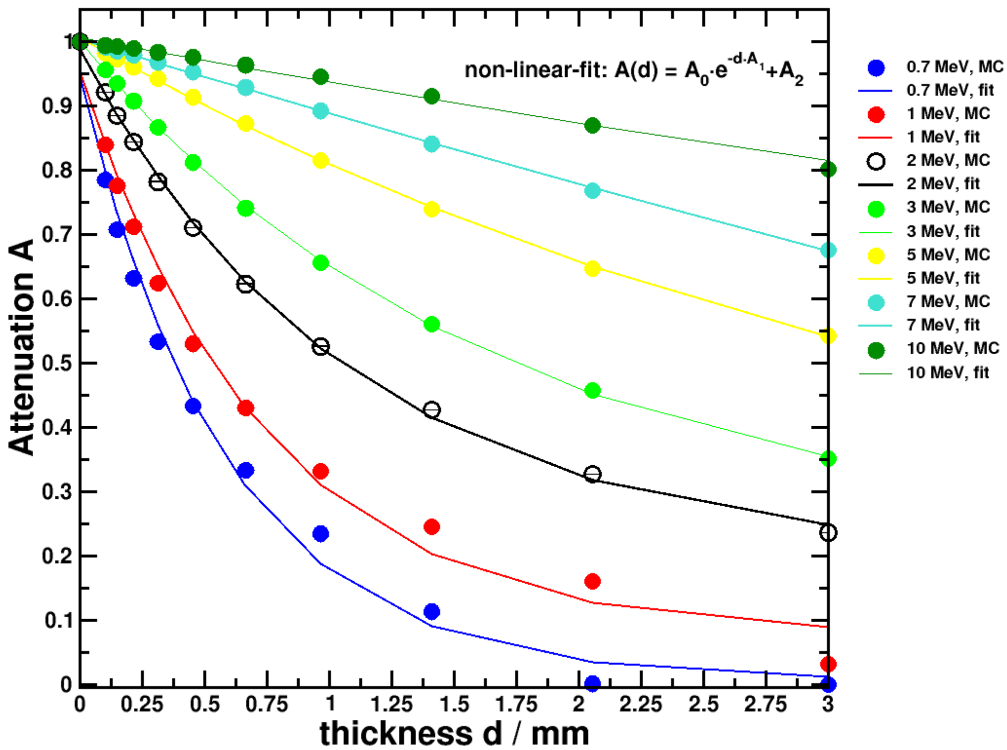

Figure 20. Attenuation of mono-energetic electron beam intensity in polycarbonate. Circles represent MC calculations while the lines are a fit to an analytic expression composed of an exponential term and a constant scatter component.

It is interesting to note that this model reproduces excellently the MC results at high energies while larger differences are observed at the lowest energies. This indicates that as the energy is reduced the energy-loss interactions deviate from this simplistic model. However, for the purposes of this investigation the three-parameter fit is satisfactory. These parameters are listed in Table A.3 for all energies considered in this project, to aid in numerical evaluation. An expression for the attenuation due to electrons of energies not included here can be obtained through interpolation of these parameters.

5.5 Shielding performance of eyewear – experiment

The experimental results for the six types of eyewear for the Sr-90 beam (as obtained using the geometry of Figure 5) are shown in Figure 21.

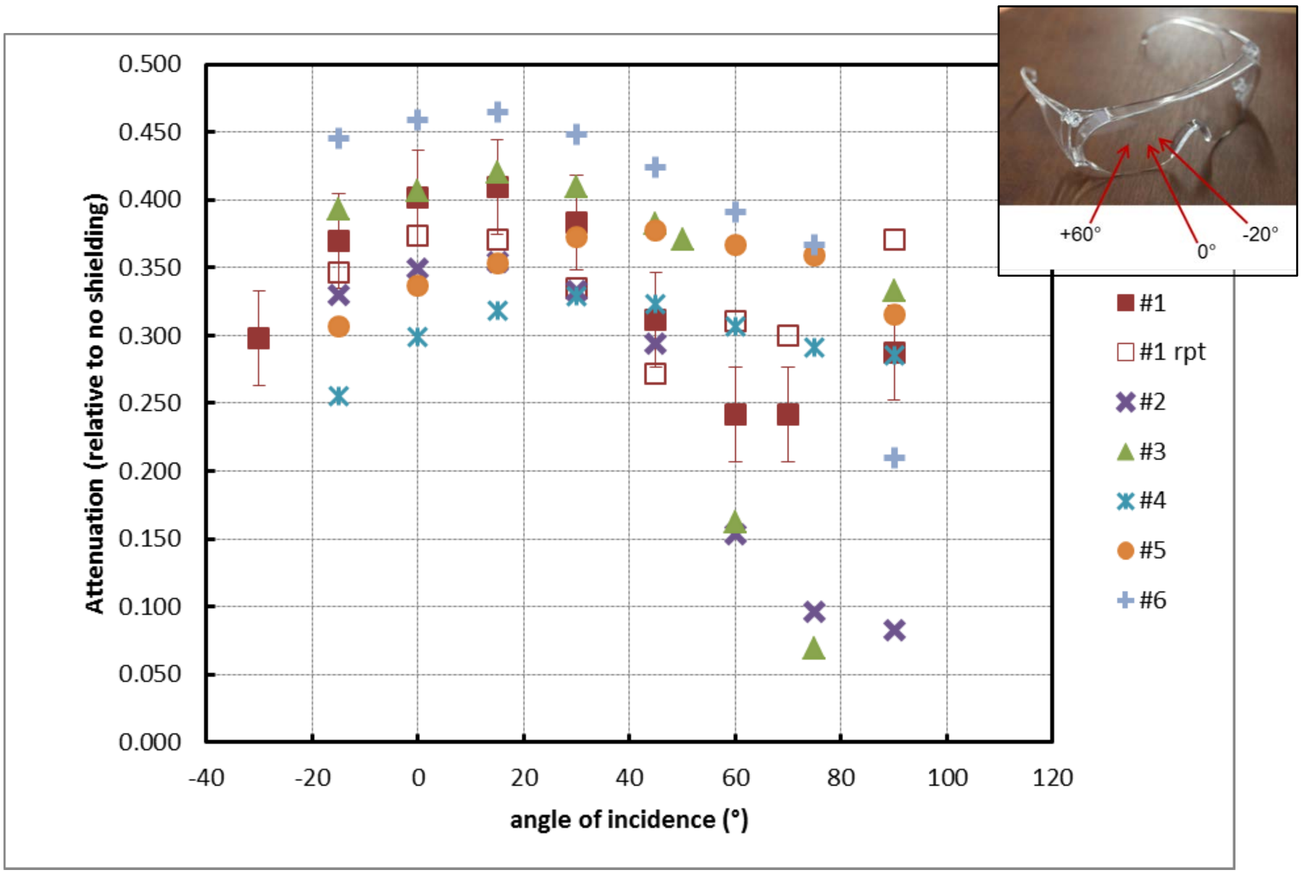

Figure 21. Results of eyewear shielding measurements using the Sr-90 source. “0” degrees corresponds to the source centred on the lens with the radiation beam axis perpendicular to the surface of the lens. Given the differing curvature of each type of eyewear, the uncertainty in setting this reference position is estimated to be 10°. The uncertainty bars are estimated from repeat measurements for planar sheets and are consistent with the difference in the two datasets for eyewear #1.

As can be seen, there are larger variations in the shielding factor (1/attenuation) between eyewear types at larger angles, where the particular design of hinge and side-pieces has a significant effect. It can be seen that eyewear #2 provides the best side protection (but with an associated loss of peripheral vision). In the central part of the eyewear lens the variation is relatively small, with shielding factors in the range 2.2 to 3.3. This variation is consistent with the different thicknesses reported in Table III.

For the kV measurements, there was little variation of the attenuation with angle. Figure 22 shows the data for eyewear #2 and Table VIII summarizes the shielding factor for the zero-degree situation for all eyewear types for the four x-ray energies.

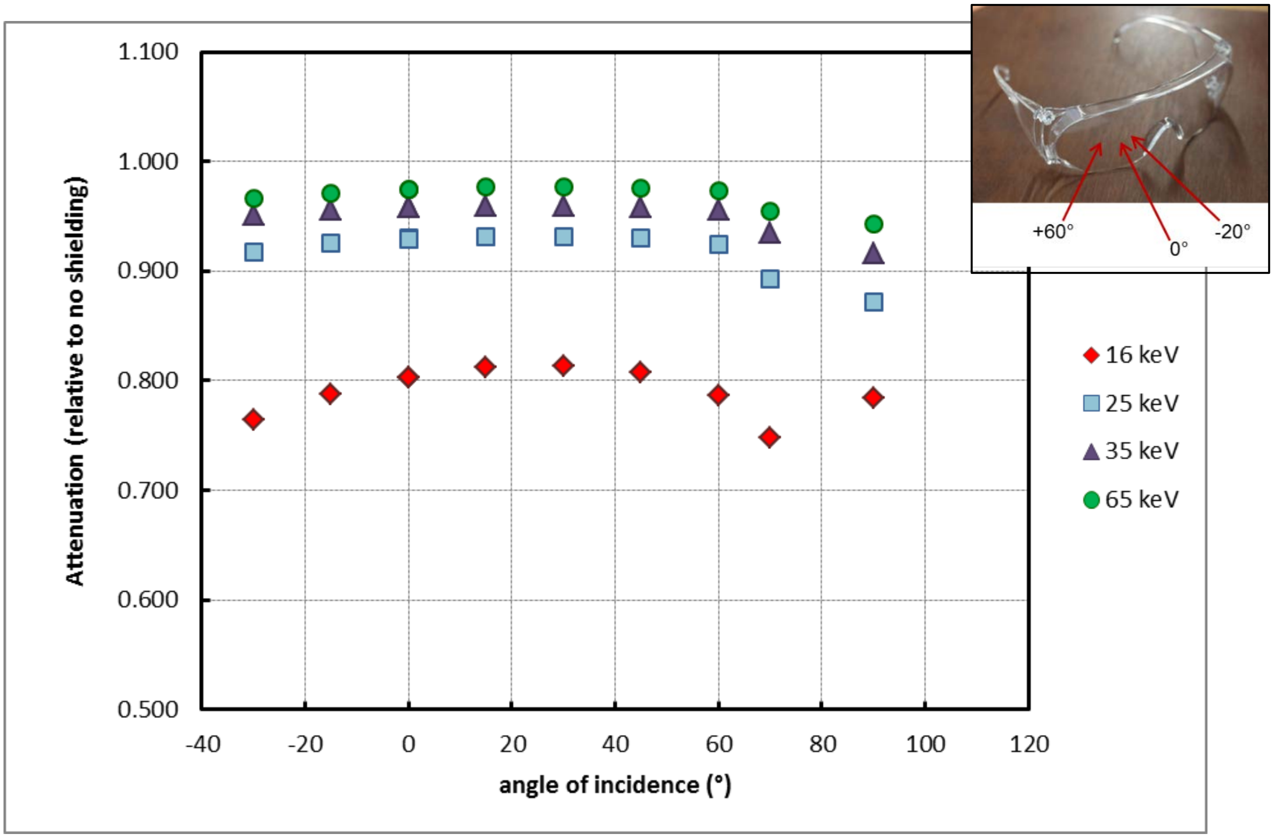

Figure 22. Attenuation in kV x-ray beams as a function of angle for eyewear #2. The data for other chamber types were qualitatively the same.

Table VIII. Summary of shielding factors for centre of eyewear lens – kV x-ray beams

Eyewear type	Effective photon energy (keV)			
	64.8	35.4	25.0	15.7
	Shielding factor (relative to no shielding)			
#1	1.03	1.04	1.07	1.24
#2	1.03	1.04	1.08	1.25
#3	1.03	1.05	1.08	1.26
#4	1.04	1.06	1.10	1.32
#5	1.03	1.05	1.09	1.27
#6	1.03	1.04	1.08	1.24
Mean	1.031	1.048	1.082	1.261
Std dev	0.5%	0.6%	1.0%	2.3%

As can be seen, the variation in the shielding factor between eyewear types for the centre part of the plastic lens is very small and, at least for those investigated here, all six types can be treated as a single type for radiation protection purposes.

5.6 Shielding performance of eyewear - simulation

The simplified Monte Carlo simulations serve as supporting evidence for the measurements described above. Comparison of the attenuation of kV x-ray beams passing through two eyewear models (cylindrical and spherical, Figure 12) as a function of the angle shows almost no difference, as seen in Figure 23. Note that rotation here means rotating the glasses around the chamber's axis of symmetry.

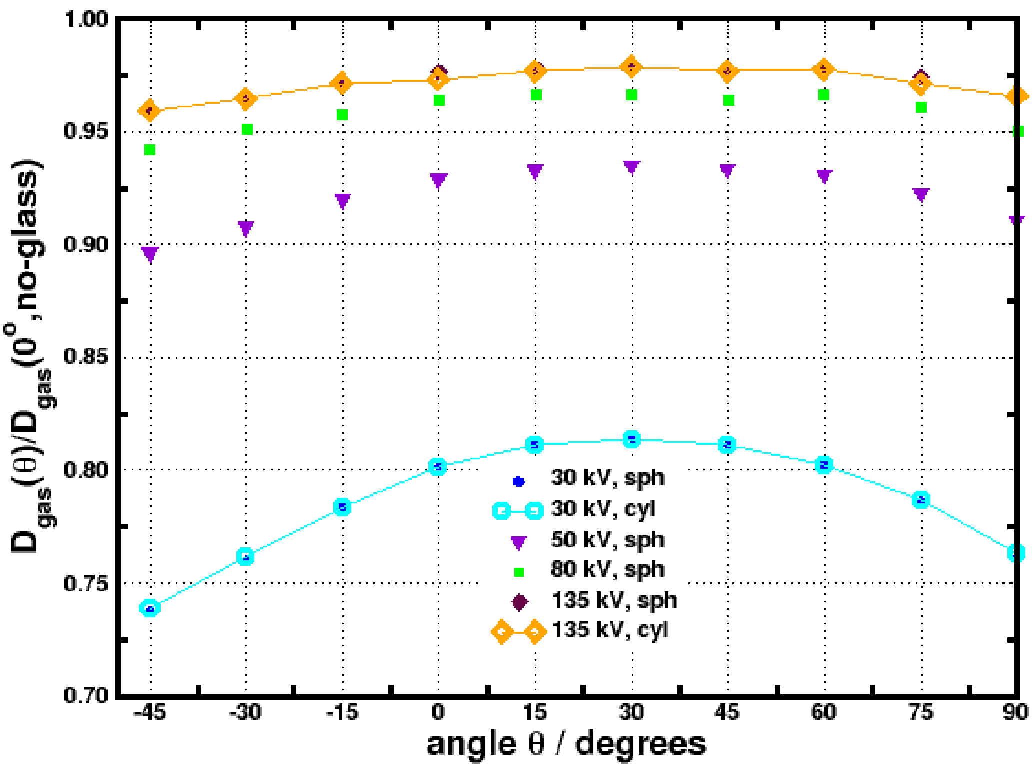

Figure 23. Comparison of the kV beam attenuation by the spherical and the cylindrical MC eyewear models. The "kV" values refer to the generating potential, see Table VI. The angle values have the same definition as for Figures 21 and 22.

It is interesting to compare these results with the experimental results and assess how well these simple geometries can reproduce the measured attenuation for real eyewear types. Figure 24 shows such a comparison between the spherical MC model and eyewear type #3. For the lowest energy beam one sees the sensitivity to the glasses design. As indicated in Table III, the lens thickness of the actual eyewear is not constant and so the differences between measurements and Monte Carlo seen in Figure 24 are most-likely due to that variation not being taken into account in the simplified simulation geometry. Non-plastic components not simulated such as nosepieces and hinges will also impact the level of agreement possible between measurement and calculation.

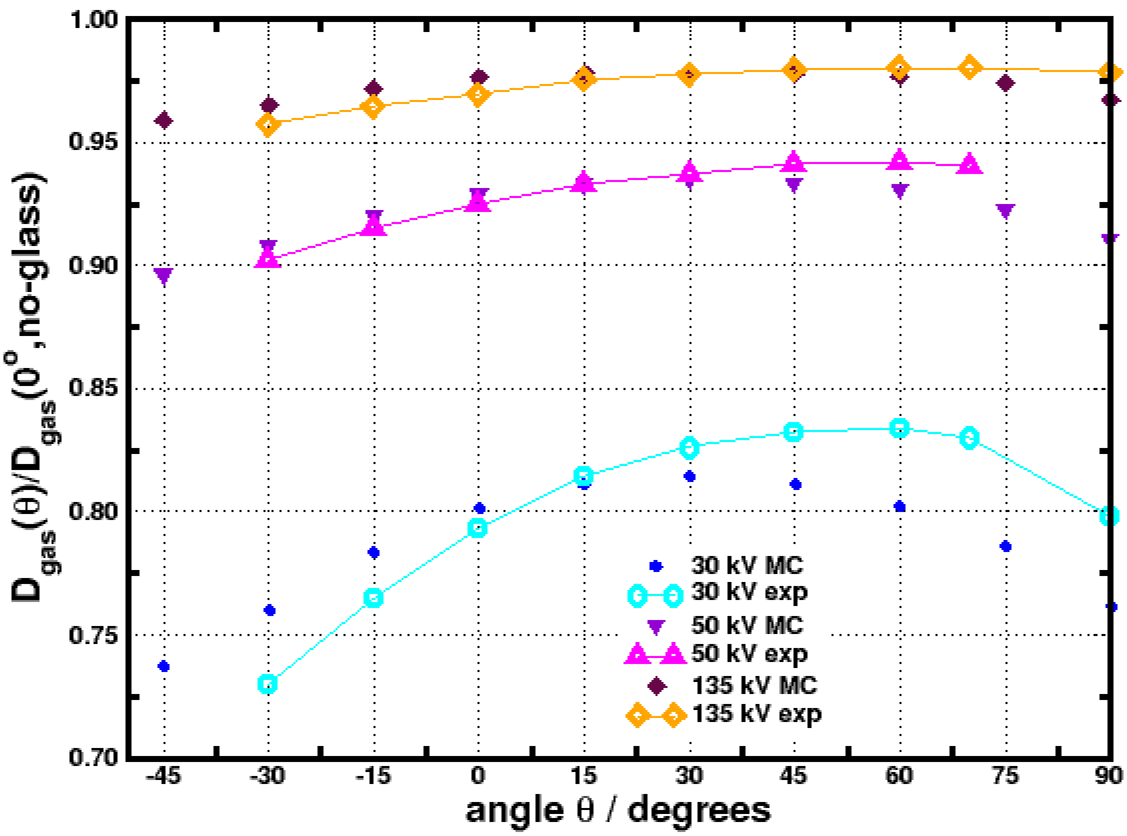

Figure 24. Comparison of the kV beam attenuation by the spherical MC model and the eyewear type #3.

Angular attenuation effects were also determined for both MC eyewear models in the Sr-90 beam; in this case the source was rotated around the chamber axis. Computation resources were a limiting factor for these calculations: 50 billion histories were required to produce a statistical uncertainty of better than 1 %. As can be seen from Fig. 25, there was little difference within uncertainties between the two simulated geometries, cylindrical and spherical. As for the x-ray simulations, there was significantly less variation in the attenuation with angle, due to the fact that the lens thickness was not modelled. The attenuation determined in the simulations at angle of 0 degrees is similar to that for eyewear type #3, which is consistent with the data in Figure 24 for x-ray beams.

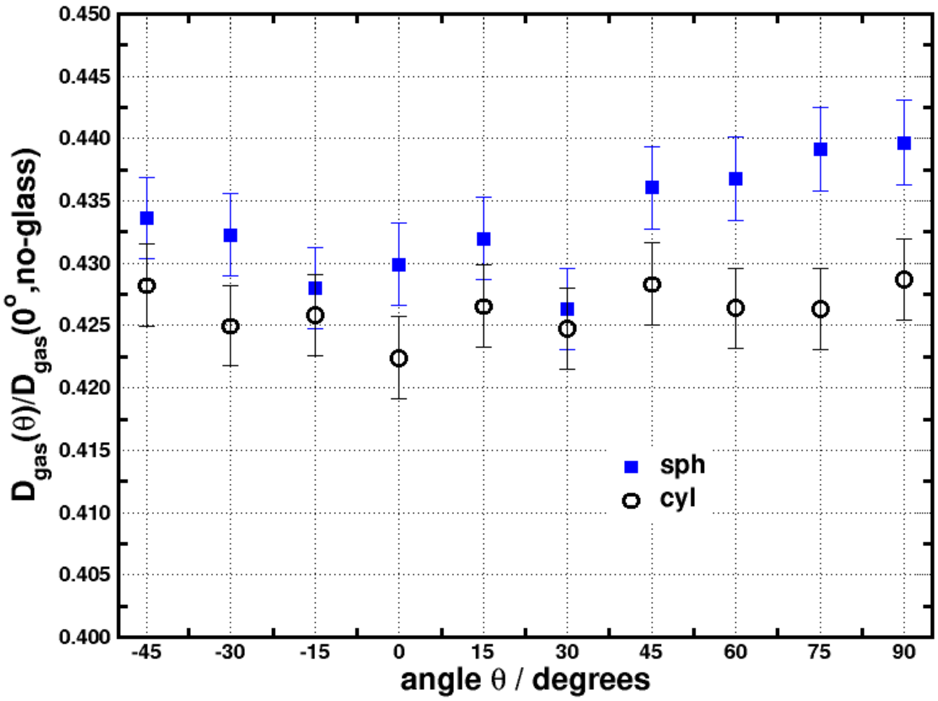

Figure 25. Comparison of the Sr-90 beam attenuation by the spherical and the cylindrical MC eyewear models. The angle values have the same definition as for Figures 21 and 22.

6. CONCLUSIONS

Data have been obtained for a range of eyewear types in a number of different photon and electron radiation beams. It is clear from the data presented in Figures 21 and 22 and in Table VIII, that the shielding factor provided by standard protective eyewear is generally very small. For a 16 keV (30 kVp) beam this factor is around 1.2, decreasing to unity as the mean photon energy approaches 100 keV. The shielding factor of the Sr-90/Y-90 beam is more significant, around 2.2-3.3 for the eyewear types tested.

At the outset of the project there was the obvious concern that the shielding factors would be very dependent on the type of eyewear (and to a lesser extent, the specific plastic shielding material). Without a wide-ranging survey of end-users, it was only possible to select enough eyewear types to cover the likely range of those found in the field. The positive finding of the study is that very little variation was found between the very different eyewear types tested. Given the precision of the measurements, and the different geometries of the eyewear types, there were measurable differences in the attenuation properties as a function of angle but, in general, the biggest type-to-type variation in shielding factor was due to the thickness of shielding material used for the eyewear lenses. No significant difference was seen in the shielding properties of the three materials tested – polycarbonate, CR-39 and Trivex – which is perhaps not surprising considering they are all low-Z polymers with similar densities.

This investigation was limited to the determination of linear attenuation using a geometry that was ideal for such a measurement (what might be described as the “classic” source-absorber-detector geometry). Angular measurements were only made in one plane and there was no attempt to simulate a realistic situation where i) the dose to both eyes is a concern and ii) the head of the wearer will likely have a significant effect in terms of either providing additional shielding or creating additional scatter dose (particularly the eye socket, which has a high density and is very close to the eye). In addition, the low activity Sr-90/Y-90 sources available created an experimental challenge, with the requirement to accurately measure sub-pA ionization currents.

It is reasonable, therefore to question whether the shielding factors obtained in this investigation apply in “real life”. The first point is that multiple investigations were carried out, using different experimental geometries and comparing measurement data with very detailed Monte Carlo simulations, to confirm the validity of the data obtained. Sensitivity studies also indicated that the attenuation measurements were generalizable to more realistic geometries (specifically larger source-detector distances). The second point is that comparisons presented above are insensitive to such issues, so the relative performance of the different materials and eyewear types remain valid independent of the irradiation geometry.

However, the excellent agreement between measurements and Monte Carlo simulations provides a basis for more complex investigations mimicking realistic radiation protection scenarios. Although anthropomorphic phantoms are available for physical dose measurements, the flexibility that the Monte Carlo approach provides, in terms of varying geometries, material compositions and incident beam energy, makes it the preferred option. The EGSnrc system used in these investigations is capable of building complex beam geometries incorporating standard CT data and it has also been used for large-scale radiation shielding simulations, so therefore one could envisage an investigation combining realistic environments, non-ideal sources (e.g. mixed radionuclides, extended sources, *etc*), accurate 3-D models of eyewear types and the dose to the lens of the eye being directly scored. This would also enable an estimate of the effect of backscatter on the dose to the lens of the eye. For electron and low-energy x-ray beams, backscattered radiation can be significant and this project did not investigate the effect. Given the anatomy behind the lens, the dose enhancement due to backscatter is worthy of further investigation.

Appendix A – additional data obtained during this investigation

Additional data and results are presented here to provide evidence for statements made in the main text. These are not included in the main text to simplify the discussion there.

Table A.1. Comparison of material attenuation in Sr-90 field.

Material	Thickness (mm)	Mass thickness ($g\ cm^{-2}$)	Shielding factor
Poly	3.48	4.00	4.5
CR-39	3.24	4.12	4.5
TVX31	3.23	3.46	3.0

Mass thickness = physical thickness x physical density

Table A.2. Variation in shielding factor due to position of 3.45 mm absorber relative to detector, source-detector distance maintained at 50 mm. Geometry as in Figure 4.

d[1] (mm)	$I_{chamber}$ (pA)	Shielding factor
---[2]	0.357	1.0
41	0.047	7.7
31	0.062	5.6
23	0.073	4.8
9	0.080	4.4

[1] distance between 3.45 mm sheet of polycarbonate and the centre of the IBA FC65-G ionization chamber

[2] measurement without any absorber present

Table A.3. Simple model parameters used to fit MC attenuation values as a function of the material thickness. See section 5.4.3 for details. Extrapolation of these parameters beyond the energy range presented is not recommended.

Energy / MeV	A_0	A_1	A_2
0.7	0.9389	1.7129	0.0072
0.8	0.9195	1.5254	0.0252
0.9	0.9007	1.4166	0.0466
1.0	0.8795	1.3647	0.0743
1.5	0.8040	1.1755	0.1743
2.0	0.7883	0.9222	0.1993
2.5	0.7770	0.7423	0.2177
3.0	0.7690	0.6075	0.2307
3.5	0.7699	0.4969	0.2329
4.0	0.7837	0.4037	0.2208
4.5	0.8156	0.3232	0.1894
5.0	0.8720	0.2542	0.1333
6.0	1.1490	0.1392	-0.1445
7.0	2.5250	0.0466	-1.5215
8.0	4.9458	0.0192	-3.9416
9.0	7.0848	0.0112	-6.0805
10.0	8.6223	0.0077	-7.6178